Title

Automated, patient-specific estimation of regional imparted energy and dose from tube current modulated computed tomography exams across 13 protocols

Journal

Journal of Medical Imaging, 4(1)

ISSN

2329-4302

Authors

Sanders, Jeremiah
Tian, Xiaoyu
Segars, William Paul
et al.

Publication Date

2017-01-24

DOI

10.1117/1.jmi.4.1.013503

Peer reviewed

Journal of Medical Imaging

MedicalImaging.SPIEDigitalLibrary.org

Automated, patient-specific estimation of regional imparted energy and dose from tube current modulated computed tomography exams across 13 protocols

Jeremiah Sanders
Xiaoyu Tian
William Paul Segars
John Boone
Ehsan Samei

Jeremiah Sanders, Xiaoyu Tian, William Paul Segars, John Boone, Ehsan Samei, "Automated, patient-specific estimation of regional imparted energy and dose from tube current modulated computed tomography exams across 13 protocols," *J. Med. Imag.* **4**(1), 013503 (2017), doi: 10.1117/1.JMI.4.1.013503.

SPIE.

Automated, patient-specific estimation of regional imparted energy and dose from tube current modulated computed tomography exams across 13 protocols

Jeremiah Sanders,[a,b,c,*] Xiaoyu Tian,[c,d] William Paul Segars,[a,c,e] John Boone,[f] and Ehsan Samei[a,b,c,d,e,g]
[a]Duke University, Medical Physics Graduate Program, 2424 Erwin Road, Suite 101, Durham, North Carolina 27705, United States
[b]Duke University, Clinical Imaging Physics Group, 2424 Erwin Road, Suite 302, Durham, North Carolina 27705, United States
[c]Duke University, Carl E. Ravin Advanced Imaging Laboratories, 2424 Erwin Road, Suite 302, Durham, North Carolina 27705, United States
[d]Duke University, Department of Biomedical Engineering, 101 Science Drive, Campus Box 90281, Durham, North Carolina 27708, United States
[e]Duke University, Department of Radiology, 2301 Erwin Road, Box 3808, Durham, North Carolina 27710, United States
[f]University of California Davis, Departments of Radiology and Biomedical Engineering, Engineering, 451 Health Sciences Drive, GBSF Room 2303, Davis, California 95616, United States
[g]Duke University, Departments of Physics and Electrical and Computer Engineering, 2424 Erwin Road, Suite 302, Durham, North Carolina 27705, United States

Abstract. Currently, computed tomography (CT) dosimetry relies on surrogates for dose, such as CT dose index and size-specific dose estimates, rather than dose *per se*. Organ dose is considered as the gold standard for radiation dosimetry. However, organ dose estimation requires precise knowledge of organ locations. Regional imparted energy and dose can also be used to quantify radiation burden and are beneficial because they do not require knowledge of organ size or location. This work investigated an automated technique to retrospectively estimate the imparted energy from tube current-modulated (TCM) CT exams across 13 protocols. Monte Carlo simulations of various head and body TCM CT examinations across various tube potentials and TCM strengths were performed on 58 adult computational extended cardiac-torso phantoms to develop relationships between scanned mass and imparted energy normalized by dose length product. Results from the Monte Carlo simulations indicate that normalized imparted energy increases with increasing both scanned mass and tube potential, but it is relatively unaffected by the strength of the TCM. The automated algorithm was tested on 40 clinical datasets with a 98% success rate. [DOI: 10.1117/1.JMI.4.1.013503]

Keywords: regional imparted energy; regional dose; patient specific; computed tomography.

Paper 16070PRR received Apr. 27, 2016; accepted for publication Dec. 29, 2016; published online Jan. 24, 2017.

1 Introduction

Current methods for computed tomography (CT) dosimetry are reliant on computed tomography dose index (CTDI) and size-specific dose estimates (SSDE). However, CTDI and SSDE are surrogates for dose rather than dose *per se*. Organ dose is a better metric for quantifying radiation burden. However, organ dose estimation requires precise knowledge of the size and location of each organ. Thus, organ dose is not a practical metric for use in the daily clinical environment. Regional imparted energy, defined as the net imparted energy to a specific region of the body in a CT exam, is another metric that can be used to evaluate radiation burden. Estimating the imparted energy instead of organ dose is simpler because it does not require precise estimates of the organ size or location. As such, it is a more practical metric to use for daily clinical dosimetry purposes.

Modern scanners come with a variety of settings that can be adjusted in performing the CT exam which ultimately determine the amount of dose the patient receives. Peak tube voltage (kV) and tube current modulation (TCM) are two of the main settings. Increasing the kV leads to a higher dose to the patient.[1] Moreover, TCM has the potential to both reduce organ dose[2] for some organs and influence image quality.[3] The strength of the TCM impacts the level of dose reduction and image quality. The precise combination of kV and TCM strength will ultimately determine the amount of radiation dose the patient will receive.

Recognizing the potential for simplification in quantifying radiation burden by estimating the imparted energy to patients undergoing CT exams, we developed an automated technique to estimate the regional imparted energy in TCM CT exams. The method is unique in that it is patient specific and protocol specific. That is, it can be used to estimate the imparted energy associated with every noncontrast-enhanced CT exam performed in the hospital that utilizes one of the 13 protocols investigated.

2 Derivation of Mass-Imparted Energy Dependency

2.1 *Modeling a Patient Population*

A library of 58 adult anthropomorphic computational extended cardiac-torso (XCAT) phantoms was used in this study.[4] This library consists of 35 males and 23 females with body mass indices ranging from 19.2 to 36.1 and 18.2 to 36.7, respectively. The

*Address all correspondence to: Jeremiah Sanders, E-mail: jeremiah.sanders@duke.edu

2329-4302/2017/$25.00 © 2017 SPIE

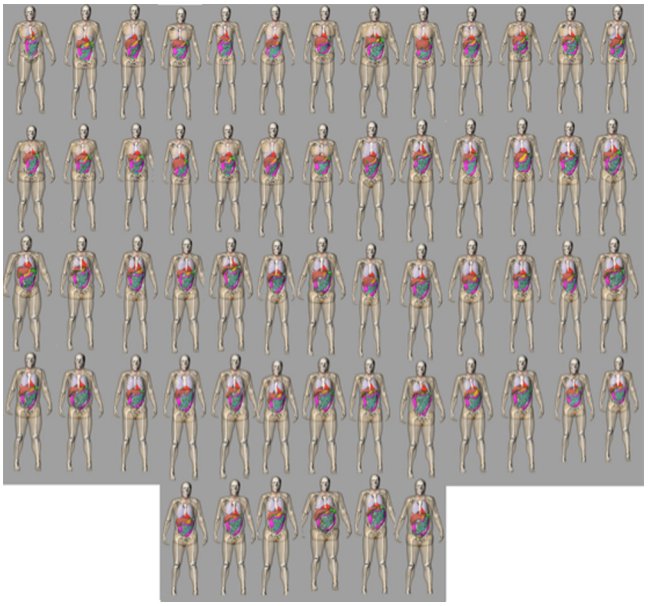

Fig. 1 The library of 58 anthropomorphic phantoms used in this study.

phantoms were modeled from clinical CT exams. All the major organs of the body were modeled in each phantom. The tissues in the phantoms are classified as lung, bone, or soft tissue with associated densities of 0.26, 1.40, and 1.03 g/cm^3, respectively.[5] The library of phantoms can be seen in Fig. 1. More detailed information regarding the phantoms can be found in Ref. 4.

2.2 *Modeling Tube Current Modulated*

Manufacturers of modern CT scanners use proprietary techniques to compute the TCM profile for a given CT exam. This makes it difficult to precisely model the TCM profile in our Monte Carlo simulations. However, a theoretical method has been devised to estimate the TCM profile based on an examination of the attenuation properties of the phantom along the length of the scan at different gantry angles.[6] For a given projection, the tube current is modeled as

$$mA = \beta A^{\alpha}, \tag{1}$$

where mA is the tube current, β is a proportionality constant, A is the attenuation through the patient, and α is the strength of the modulation. A ray-tracing algorithm was used to determine the attenuation through the phantom at a given projection. The collection of mA values for the various projections makes up the TCM profile. A detailed description of the algorithm is outlined by Li et al.[6]

Various TCM strengths were investigated in this study ($\alpha = 0.00$, 0.25, 0.50, 0.75, and 1.00). The strength of the TCM can vary from zero, corresponding to fixed tube current, to one, corresponding to maximum modulation as a function of attenuation. The value for the TCM strength is reflective of different CT implementations and can be adjusted on certain scanners. As the TCM strength is increased, the noise properties in each projection vary. Constant noise across all projections can be achieved with $\alpha = 1.00$.[3] An example set of TCM profiles generated for an abdominopelvic scan at 120 kV is shown in Fig. 2.

2.3 *Modeling Dose*

A validated PENELOPE-based Monte Carlo program was used in this study.[7] Li et al. demonstrated that discrepancies between simulation and measurement ranged between −17% and 13% for helical scans simulated with this program. The inputs to the program were the computational XCAT phantoms, TCM profiles, x-ray spectrum, and input files defining beam collimation, phantom positioning in the bore of the scanner, number of photon histories, source to isocenter distance, and start and stop locations for the scan. A summary of the main input parameters for simulating a Siemens Definition Flash scanner is provided in Table 1.

The output of the PENELOPE simulation was a three-dimensional (3-D) dose profile per 100 mAs of the phantom. An example is shown in Fig. 3(b). Each voxel of the 3-D dose profile contained the dose to that voxel, defined as the imparted energy to the voxel divided by the mass of the voxel. This is expressed mathematically as

$$D = \frac{\varepsilon}{m}, \tag{2}$$

where D is the dose, ε is the imparted energy, and m is the mass. The mass of voxels can be found by multiplying the density ρ of the tissue contained in each voxel by the volume V of the voxel, i.e., $m = \rho V$. Thus, one can isolate the imparted energy to the voxel by multiplying both sides of Eq. (2) by the mass m.

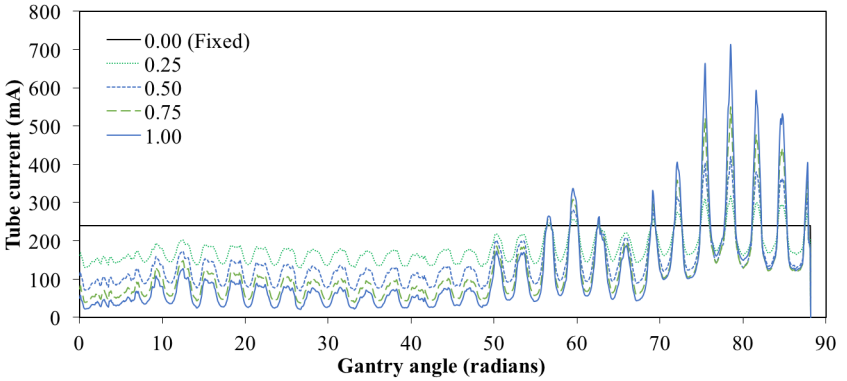

Fig. 2 An example set of TCM profiles generated for a 120 kV abdominopelvic exam.

Table 1 Main input parameters for the Monte Carlo simulations emulating a Siemens Definition Flash scanner.

Parameter	Value
Number of photon histories	5×10^8
Pitch	0.8
Fan angle	25°
Collimation	38.4 mm
Effective beam width	44.4 mm
Source to isocenter distance	59.5 cm
Tube potential	80, 100, 120, and 140 kV

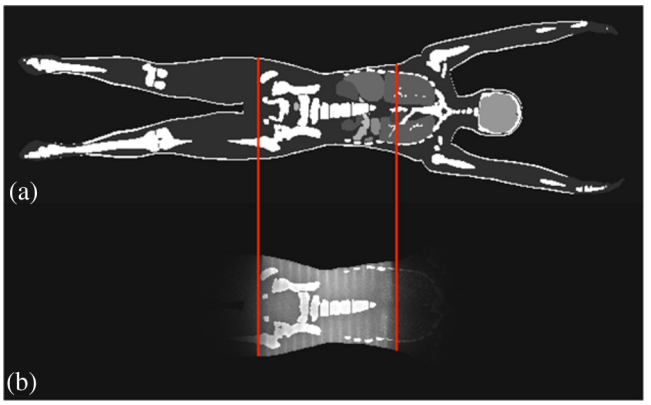

Fig. 3 (a) A cross section of one of the XCAT phantoms showing details of anatomical structures. (b) An example dose profile generated from a PENELOPE simulation of an abdominopelvic exam performed on the phantom in (a) using a 120 kV tube potential. The red lines indicate the scan region that was defined.

The net imparted energy to the phantom normalized by DLP for a given examination was the target of this study. Normalizing by DLP allows the results to be used for multiple scanners and protocols as the $\mathrm{CTDI_{vol}}$ can serve as a normalizer across such dependencies. The method used here for simulating $\mathrm{CTDI_{vol}}$ is described by Tian et al.[8] The normalized net imparted energy can be computed as the sum of the imparted energy to all voxels within the phantom, including the voxels containing scattered radiation divided by the DLP of the exam. This is expressed as

$$\frac{\varepsilon_{\mathrm{net}}}{\mathrm{DLP}} = \frac{\sum_{k=1}^{n}\sum_{j=1}^{m}\sum_{i=1}^{l}\varepsilon_{i,j,k}}{L \cdot \mathrm{CTDI_{vol}}}, \tag{3}$$

where $\varepsilon_{\mathrm{net}}$ is the net imparted energy to the phantom, $\varepsilon_{i,j,k}$ is the imparted energy to the voxel with indices i, j, k, and L is the scan length. Since both $\varepsilon_{\mathrm{net}}$ and $\mathrm{CTDI_{vol}}$ are per 100 mAs, the normalization by 100 mAs cancels out in Eq. (3).

2.4 *Mass-Imparted Energy Database*

The normalized imparted energy was computed for each of the 58 XCAT phantoms under 13 different scan protocols using four kV settings (80, 100, 120, and 140 kV) and the five TCM strengths listed above. The $\mathrm{CTDI_{vol}}$ values for the four different kV settings were 2.050, 4.191, 7.025, and 10.168 mGy/100 mAs, respectively. The 13 scan protocols are defined in Table 2. The mass of the scanned region of the phantoms was also calculated by finding the net mass of tissue in-between the start and stop regions of each protocol. These data were used to generate a database of the normalized imparted energy as a function of the scanned mass for each protocol and scan setting. A knowledgebase was extracted from the database by applying second-order polynomial fits to each dataset in the database. These fit lines were used in the step below to estimate the imparted energy to actual patients based on an estimate of the scanned mass from their CT dataset. The equation used for the fit lines was

$$\frac{\varepsilon_{\mathrm{net}}}{\mathrm{DLP}} = c_1 M^2 + c_2 M + c_3, \tag{4}$$

where c_1, c_2, and c_3 are coefficients, and M is the scanned mass.

Table 2 Definitions of the scan regions for the 13 different protocols.[9]

Region	Protocol	Start location	Stop location
Body	Abdomen	1 cm above superior liver	1 cm below inferior iliac crest
	Abdomen–pelvis	1 cm above superior liver	1 cm below inferior ischium
	Adrenal	1 cm above superior adrenals	1 cm below inferior adrenals
	Chest	1 cm above lung apex	1 cm below lung base
	Chest–abdomen–pelvis	1 cm above lung apex	1 cm below inferior ischium
	Kidney	1 cm above superior kidneys	1 cm below inferior kidneys
	Kidney–bladder	1 cm above superior kidneys	1 cm below inferior bladder
	Liver	1 cm above superior liver	1 cm below inferior liver
	Liver–kidney	1 cm above superior liver	1 cm below inferior kidneys
	Pelvis	1 cm above superior iliac crest	1 cm below inferior ischium
Head	Head	1 cm above top of skull	1 cm below base of skull
	Head–neck	1 cm above top of skull	1 cm below inferior C7 vertebrae
	Neck	1 cm above superior C1 vertebrae	1 cm below inferior C7 vertebrae

3 Regional Imparted Energy Estimation from Clinical Computed Tomography Datasets

3.1 *Mesh Generation and Scanned Mass Estimation for Clinical Exams*

This point marks the transition from the work on the XCAT phantoms to the work on the clinical CT datasets. A program was devised to segment the patient's body from their clinical dataset using a multithreshold technique.[10] Since the cushion patients lie on has a similar Hounsfield unit (HU) to skin, it often times poses a challenge for the segmentation. Thus, passing the dataset through multiple thresholds helps remove the cushion from the segmentation mask. Seven thresholds were selected by manually finding the optimal thresholds from a database of CT images that were unrelated to this study. The dataset was passed through the thresholds to create a binary volume of the patient's soft tissue. A morphological hole-filling operation was applied to fill in the lower density regions inside the patient. The result was a binary volume representing the patient's body.

An MATLAB-based open source mesh generation toolbox, iso2mesh, was used to reconstruct the contour of the scanned region of the patient from their CT dataset.[11] The "v2m" function in the toolbox was used for this purpose. It requires the binary volume of the patient along with user-defined constants, including the size of the mesh. A mesh size of 4 was used in this study. The outputs of the v2m function that were used were the node coordinates and list of elements that make up the tetrahedral mesh. A few examples of reconstructed volumes from head, chest, and abdominopelvic exams are shown in Fig. 4. An additional function, "elemvolume," was used to determine the volume of each element in the tetrahedral mesh. All the individual element volumes were then summed to compute the total volume of the scanned region.

To estimate the scanned mass of the patient, the volume calculation from the previous step is multiplied by an effective density. The effective density is defined as a weighted sum of the individual densities: bone, soft tissue, lung, and air. Air in the patient, such as within the esophagus or gas pockets in the gastrointestinal track, was subtracted out as it does not contribute to the mass of the patient. An effective density was derived as

$$\rho_{\text{eff}} = W_{\text{B}}\rho_{\text{B}} + W_{\text{ST}}\rho_{\text{ST}} + W_{\text{L}}\rho_{\text{L}} - W_{\text{A}}\rho_{\text{A}}, \tag{5}$$

where ρ_{eff} is the effective density, W_{B}, W_{ST}, W_{L}, and W_{A} are the weighting factors for bone, soft tissue, lung tissue, and air, respectively, and ρ_{B}, ρ_{ST}, ρ_{L}, and ρ_{A} are the densities of bone, soft tissue, lung tissue, and air, respectively. The values used were 1.4 g/cm^3 for bone, 1.03 g/cm^3 for soft tissue, 0.26 g/cm^3 for lung,[5] and 1.205×10^{-3} g/cm^3 for air.[12] The weighting factors were determined by finding the ratio of the number of "true" (or 1) voxels in the binary volume that represent a particular tissue to the total number of "true" voxels in the binary volume. For example, consider a binary volume of a patient that is segmented from a chest CT exam, containing 5,100,000 voxels label as "true." Of these voxels, 2,000,000 are identified as the lung, 2,250,000 are identified as soft tissue, 750,000 are identified as bone, and 100,000 are identified as air. The weighting factors for the lungs, soft tissue, bone, and air would be 0.392, 0.441, 0.147, and 0.020, respectively.

As the patient mass estimation is dependent on the patient volume, it is necessary to validate the accuracy of the volume estimation from the tetrahedral mesh. For this purpose, a multisized phantom (Mercury V3.0, Duke University, Durham, North California) was input into the mesh generation algorithm, and the estimated volume was compared with an analytical volume calculation. The dimensions of the Mercury Phantom are shown in Fig. 5 beside the tetrahedral mesh that was generated.

The voxels representing a particular tissue in the binary volume of the patient were classified based on the value of their HU. Otsu thresholding[13] was applied to the CT dataset using three thresholds. Performing this operation splits the histogram of the CT dataset into three sections. The three different sections represent the three major tissue types: lung, soft tissue, and bone. Binary masks of each tissue type were created with the thresholds, and the weighting factors were determined from the binary masks. The air pockets in the patient are segmented

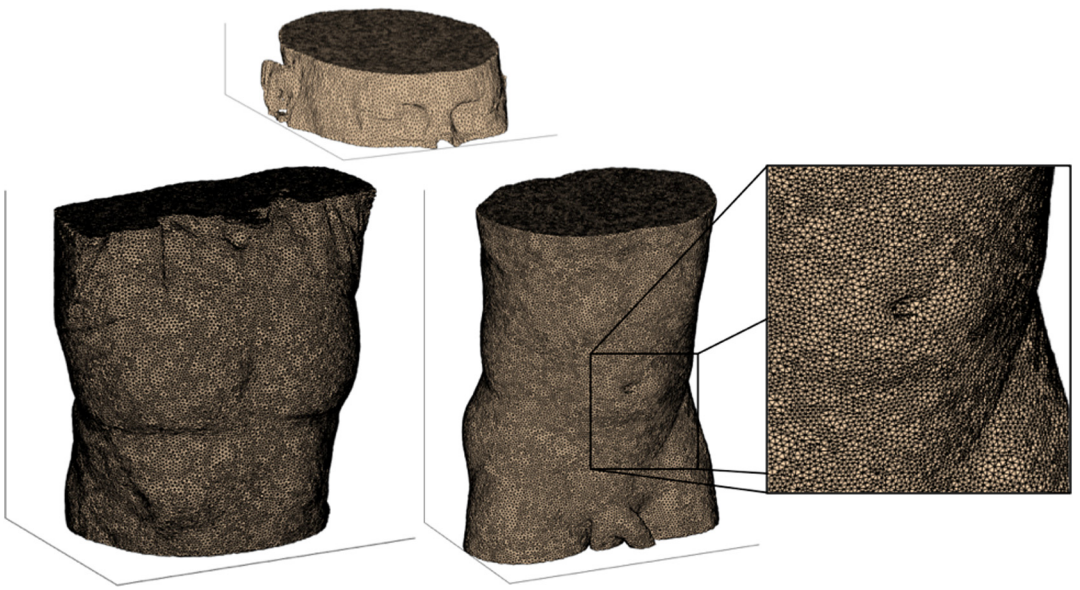

Fig. 4 An example set of volumes reconstructed from head, chest, and abdominopelvic CT datasets.

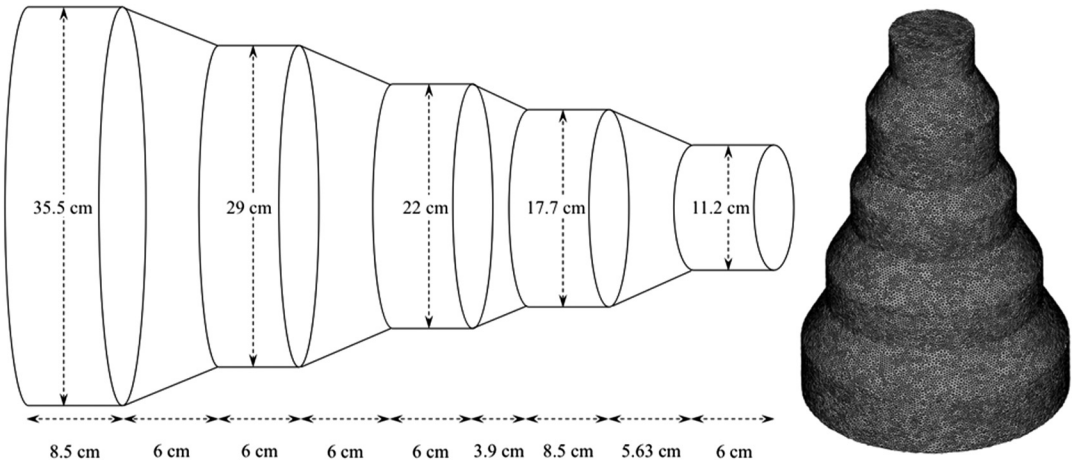

Fig. 5 The Mercury Phantom V3.0 used for validating the volume estimation from the tetrahedral mesh.

with the lungs. Most of the air pockets are much smaller than the lungs in the binary mask, so they were removed using the "bwareaopen" function in MATLAB. The larger air pockets with cross-sectional areas comparable to those of the lungs were removed based on the location of their geometric centroid relative to the center of the image. Their centroid is located further from the image center than that of the lungs.

3.2 *Patient-Specific Regional Imparted Energy Estimation*

The program was tested on 20 clinical abdominopelvic and 20 clinical chest CT datasets. The clinical datasets were anonymously obtained from Duke Hospital's database of CT exams with IRB approval, and all the clinical datasets were acquired with a 120 kV setting. First, each dataset was input into the algorithm to determine the scanned mass. Next, the estimate of the scanned mass was plugged into the equation for the normalized imparted energy corresponding to the proper protocol and kV setting. Finally, the result was multiplied by the DLP of the exam. The average and standard deviation of the imparted energy for each protocol were computed. The variation in normalized imparted energy was quantified by determining the percent change in normalized imparted energy with TCM strength with respect to fixed tube current.

4 Results

The analytically computed volume of the Mercury Phantom was 0.030 m^3. The volume of the Mercury Phantom computed by the automated algorithm was 0.029 m^3. Thus, the error in the volume estimation was 3.3%.

Figure 6 shows the results for the normalized imparted energy as a function of scanned mass for 120 kV abdominopelvic and chest simulated scans and various TCM strengths. The results from varying the strength of the TCM are presented in Fig. 7. Visual inspection of these figures reveals that the variability in normalized imparted energy with TCM strength is small, as the absolute maximum percent change in normalized imparted energy for abdominopelvic exams is 1.8%. This implies that the effect of TCM is negligible when considering the normalized net amount of energy deposited to tissue. The variation in normalized imparted energy with increasing TCM strength was investigated for the other protocols, and the highest percent change in normalized imparted energy was 2.5% corresponding to chest exams.

Figure 8 shows the results of the normalized imparted energy versus scanned mass for abdominopelvic and chest exams using various kV settings. The results shown are for fixed tube current conditions. The equations for the second-order polynomial fit lines applied to the data for this protocol and all the other

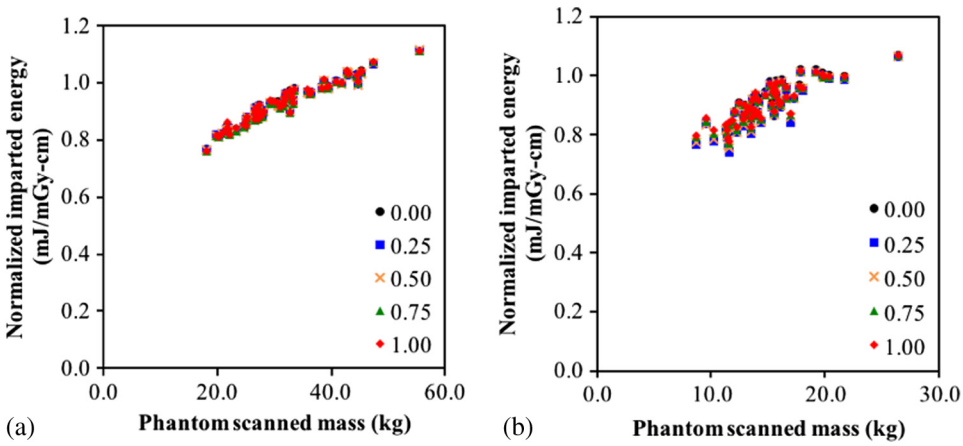

Fig. 6 Normalized imparted energy versus scanned mass for various TCM strengths. The results shown are for the 120 kV setting. (a) Abdominopelvic exams and (b) chest exams.

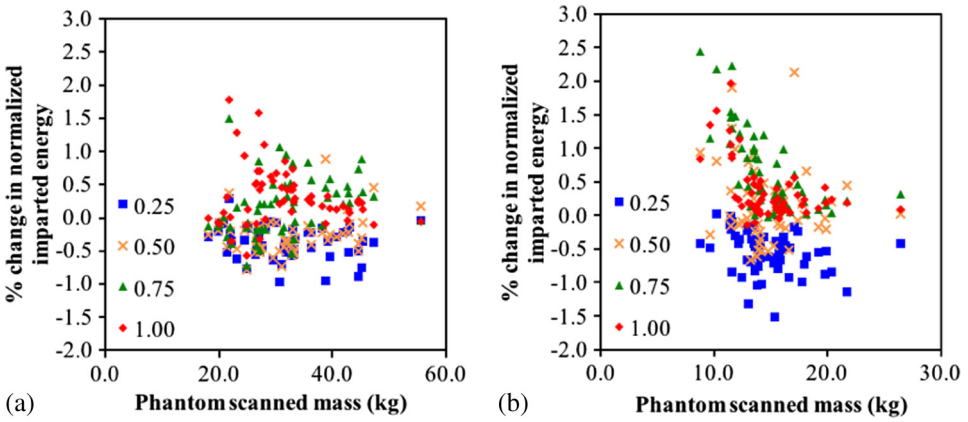

Fig. 7 Percent change in normalized imparted energy with respect to fixed tube current for various TCM strengths. Results shown are for the 120 kV setting. (a) Abdominopelvic exams and (b) chest exams.

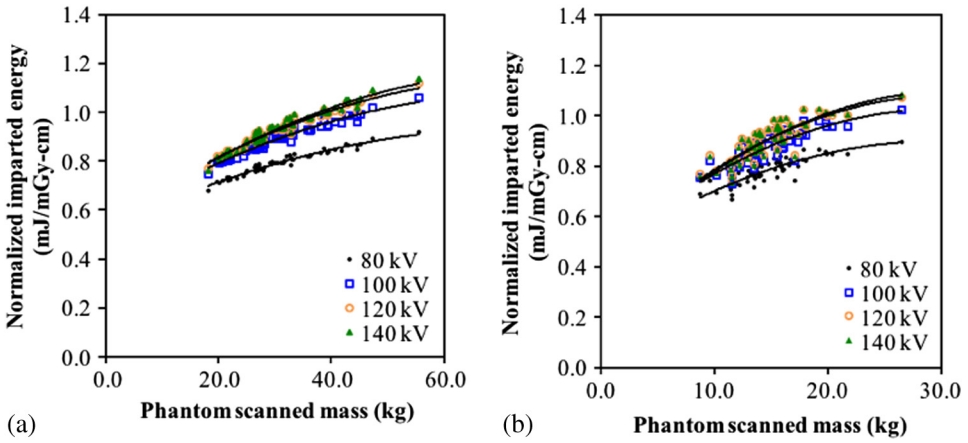

Fig. 8 Simulation results of the normalized imparted energy as a function of scanned mass for (a) abdominopelvic exams and (b) chest exams. The results shown are for fixed tube current.

protocols are summarized in Table 3. The plot shown here indicates that the normalized imparted energy increases with increasing kV. This is the expected result since patient dose increases with increasing kV, and patient dose is proportional to imparted energy for a given scan region. The increase is greatest from 80 to 100 kV and smallest from 120 to 140 kV. These same trends were observed for the other 11 protocols investigated in this study.

Figure 9 summarizes the results from testing the algorithm on 20 datasets of each protocol. The average imparted energy was 681 ± 376 mJ for abdominopelvic exams and 274 ± 141 mJ for chest exams. The program failed on one of the 40 datasets. This was due to improper placement of the patient within the bore of the CT scanner. Overall, the method provided patient-specific estimates of imparted energy for 98% of the cases tested.

5 Discussion

Organ dose has been accepted as the gold standard for radiation dosimetry purposes. However, in daily clinical practice, the use of organ dose is impractical because it requires precise estimates of organ location and size. Moreover, some organ dosimetry techniques based on Monte Carlo simulations require the patient CT data to be matched to a specific phantom with similar anatomy to the patient. Although such matching techniques are still under development, regional imparted energy can also be used to quantify radiation burden. Estimating the imparted energy instead of organ dose is beneficial because it does not require precise estimates of the organ size or location.

Currently, there is much effort by researchers to develop dose-monitoring programs due to organizations pressuring medical facilities to report CT doses on a patient-by-patient basis.[14] However, many of these programs report surrogates for dose, such as CTDI or SSDEs, rather than dose *per se*. The work in this paper presents a method to estimate the net imparted energy to a patient undergoing CT exams in specific regions of the body based on an estimate of their scanned mass. It is trivial to convert the regional imparted energy estimate to a regional dose estimate by dividing the imparted energy by the scanned mass. Doing so would provide a reportable dose estimate specific to the type of scan being performed. Additionally, regional imparted energy/dose tracking could be implemented into the clinical workflow by storing both the regional imparted energy and the regional dose estimates in patient records.

The results presented in Fig. 7 show that the strength of the TCM has a minor impact on the normalized imparted energy when compared with the fixed tube current condition. For this reason, we reported the results of the normalized imparted energy as a function of scanned mass for the fixed tube current condition only. One could expect to achieve approximately the same imparted energy estimates using the knowledgebase in

Table 3 Parameters for the fit lines applied to the data of normalized imparted energy versus scanned mass.

Protocol	kV	c_1	c_2	c_3	R^2
Abdomen	80	−0.0003	0.0202	0.5494	0.8960
	100	−0.0003	0.0251	0.5862	0.8953
	120	−0.0004	0.0278	0.5879	0.8944
	140	−0.0004	0.0292	0.5738	0.8938
Abdomen–pelvis	80	-8×10^{-5}	0.0113	0.5177	0.9609
	100	-9×10^{-5}	0.0142	0.5456	0.9604
	120	−0.0001	0.0158	0.5415	0.9598
	140	−0.0001	0.0166	0.5234	0.9591
Adrenal	80	−0.0040	0.0680	0.5920	0.5808
	100	−0.0050	0.0865	0.6354	0.5820
	120	−0.0056	0.0968	0.6400	0.5816
	140	−0.0059	0.1026	0.6271	0.5811
Chest	80	−0.0005	0.0301	0.4507	0.7263
	100	−0.0006	0.0379	0.4526	0.7274
	120	−0.0007	0.0422	0.4327	0.7284
	140	−0.0007	0.0445	0.4051	0.7290
Chest–abdomen–pelvis	80	-6×10^{-5}	0.0102	0.4631	0.9603
	100	-7×10^{-5}	0.0128	0.4727	0.9595
	120	-8×10^{-5}	0.0143	0.4574	0.9587
	140	-8×10^{-5}	0.0151	0.4328	0.9580
Kidney	80	−0.0010	0.0407	0.5289	0.8786
	100	−0.0013	0.0512	0.5601	0.8776
	120	−0.0014	0.0571	0.5578	0.8770
	140	−0.0015	0.0605	0.5408	0.8764
Kidney–bladder	80	−0.0002	0.0182	0.4871	0.9394
	100	−0.0002	0.0229	0.5071	0.9406
	120	−0.0003	0.0255	0.4982	0.9415
	140	−0.0003	0.0269	0.4772	0.9421
Liver	80	−0.0006	0.0308	0.5188	0.8218
	100	−0.0007	0.0382	0.5480	0.8253
	120	−0.0008	0.0421	0.5453	0.8278
	140	−0.0008	0.0442	0.5290	0.8299
Liver–kidney	80	−0.0003	0.0220	0.5614	0.9285
	100	−0.0004	0.0275	0.6001	0.9268
	120	−0.0004	0.0305	0.6022	0.9253
	140	−0.0005	0.0321	0.5880	0.9241
Pelvis	80	−0.0002	0.0200	0.5260	0.9585
	100	−0.0003	0.0254	0.5543	0.9603
	120	−0.0003	0.0285	0.5491	0.9611
	140	−0.0003	0.0303	0.5293	0.9614
Head	80	−0.0024	0.0664	0.1794	0.7480
	100	−0.0027	0.0760	0.1626	0.7818
	120	−0.0028	0.0793	0.1444	0.8010
	140	−0.0027	0.0796	0.1276	0.8146
Head–neck	80	−0.0016	0.0591	0.1435	0.8795
	100	−0.0018	0.0688	0.1148	0.8958
	120	−0.0019	0.0727	0.0901	0.9050
	140	−0.0019	0.0737	0.0693	0.9117
Neck	80	−0.0040	0.0933	0.2480	0.9365
	100	−0.0047	0.1105	0.2313	0.9428
	120	−0.0049	0.1180	0.2099	0.9465
	140	−0.0049	0.1204	0.1887	0.9494

Table 3 regardless of the strength of the TCM. This is supported by results obtained from Tian et al.[2] In that work, the variation of organ dose with TCM strength was investigated. The results showed that the dose to some organs, such as the stomach, decreased with increasing TCM strength, whereas the dose to other organs, such as the bladder, increased with increasing TCM strength. Since dose is proportional to imparted energy, it follows that some organs receive more imparted energy with increasing TCM strength, whereas other organs receive less imparted energy with increasing TCM strength. The net effect is that the total imparted energy to the tissue remains approximately constant.

The dependence of tube potential on effective dose normalized by DLP (ED/DLP) was investigated by Huda et al.[15] In that paper, they showed that increasing the x-ray tube voltage from 80 to 140 kV resulted in an average increase in ED/DLP of ~25% for body CT exams. This result is consistent with the results presented in this paper for body exams. However, Schlattl et al.[16] concluded that tube potential had a relatively small impact on dose conversion coefficients (DCC) in CT examinations with TCM. One possible explanation for this discrepancy is that Huda et al. and this study looked at doses in adults, whereas the study by Schlattl et al. focused on pediatrics. Moreover, Schlattl et al. examined only three phantoms in their study, and they investigate the impact of kV on DCC for a single phantom of a child. In this study, 58 phantoms were analyzed. As such, the results presented in this paper provide a more comprehensive evaluation of the impact of kV on normalized imparted energy and dose.

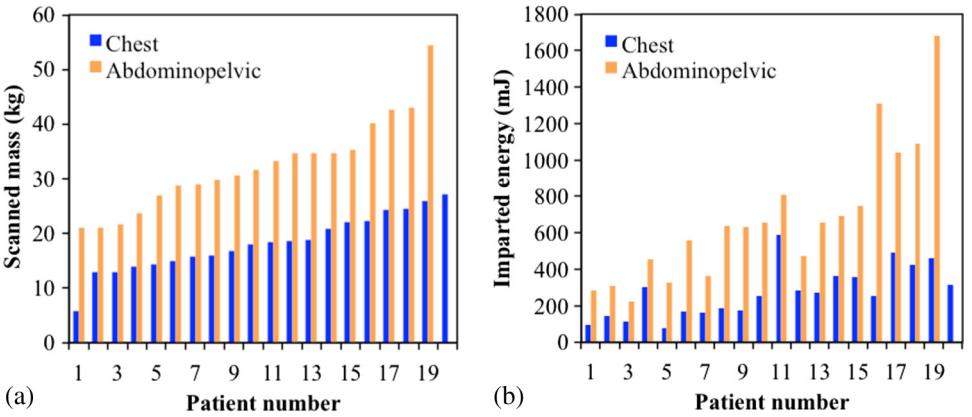

Fig. 9 (a) Scanned mass and (b) corresponding imparted energy estimates from the 20 clinical chest and 20 clinical abdominopelvic CT exams.

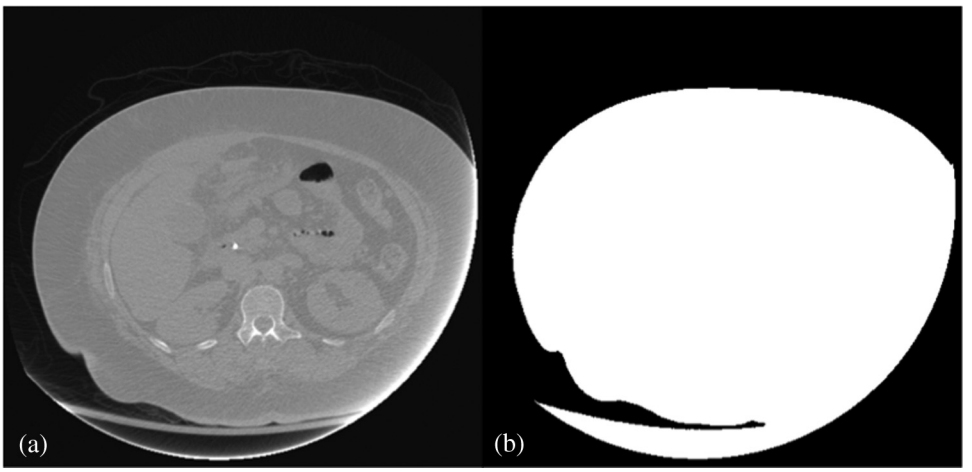

Fig. 10 (a) Image of a patient that was improperly positioned in the bore of the CT scanner. An artifact is apparent on the right side of the image. (b) Failed segmentation of the image due the artifact.

This work has several limitations. The accuracy of the imparted energy estimate is dependent on the quality of the image segmentation. In some instances, the program may fail to segment the entire patient from their CT dataset due to image artifacts or external objects in the FOV. Either way, this will ultimately lead to an inaccurate estimate of the scanned mass and thus an inaccurate estimation of the imparted energy. For particularly large patients, some of their body may lie outside of the field of view (FOV). As a result, this part of their body would not be captured in the CT dataset. Since the mass estimation is based on the information contained only in the CT dataset, the mass of the patient lying outside the FOV will not be included in the mass estimation. Along the same lines, in this study, for one case, the segmentation failed because the patient table was included in the binary volume. An artifact on the right side of the FOV artificially raised the HU of some of the voxels in-between the patient and the table, which connected the two objects together in the segmentation as shown in Fig. 10. When the segmentation fails, it leads to inaccurate estimation of the scanned mass, which propagates into an inaccurate estimation of the imparted energy to the patient.

Finally, the proprietary nature of the method in which manufacturers determine the TCM profile for a particular patient makes it difficult to validate the accuracy of TCM profiles generated from the theoretical model. The qualitative nature of manufacturers' TCM profile generation was determined by Keat.[17] However, since the results did not show a strong dependence on the TCM strength, one can conclude the slight discrepancy between actual and modeled TCM would have negligible impact on the imparted energy.

6 Conclusion

Retrospective estimates of imparted energy to patients undergoing TCM CT exams can be automatically assessed to quantify radiation burden. This was done by estimating the scanned mass of the patient from their CT dataset, and using the scanned mass and DLP of the exam to estimate the imparted energy from the knowledgebase ascertained in this study. The absolute maximum percent change in normalized imparted energy with respect to fixed tube current for all TCM strengths and protocols examined was greatest (2.5%), but still small, for chest exams. This implies that the net imparted energy is relatively unaffected by the strength of the TCM. Moreover, results indicate that the imparted energy is dependent on the kV setting, increasing with increasing kV. The accuracy of the imparted energy estimate is based on the quality of the segmentation.

Disclosures

Ehsan Samei has active research grants with General Electric and Siemens. No other conflicts of interest to disclose.

Acknowledgments

The authors would like to thank Josh Wilson, PhD, from Duke's Clinical Imaging Physics Group for helping acquire the CT datasets that were used in this study.

References

1. J. T. Bushberg et al., "Radiation dose," Chap. 13.7 in *The Essential Physics of Medical Imaging*, 2nd ed., T. DeGeorge, Ed., pp. 362–367, Lippincott Williams & Wilkins, Philadelphia, Pennsylvania (2002).
2. X. Tian et al., "Prospective estimation of organ dose in CT under tube current modulation," *Med. Phys.* **42**, 1575–1585 (2015).
3. M. Gies et al., "Dose reduction in CT by anatomically adapted tube current modulation. I. Simulation studies," *Med. Phys.* **26**, 2235–2247 (1999).
4. W. P. Segars et al., "Population of anatomically variable 4D adult phantoms for imaging research and optimization," *Med. Phys.* **40**, 043701 (2013).
5. X. Li et al., "Patient-specific radiation dose and cancer risk estimation in CT: Part II. Application to patients," *Med. Phys.* **38**, 408–419 (2011).
6. X. Li, W. P. Segars, and E. Samei, "The impact on CT dose of the variability in tube current modulation technology: a theoretical investigation," *Phys. Med. Bio.* **59**, 4525–4548 (2014).
7. X. Li et al., "Patient-specific radiation dose and cancer risk estimation in CT: Part I. Development and validation of a Monte Carlo program," *Med. Phys.* **38**, 397–407 (2011).
8. X. Tian et al., "Dose coefficients in pediatric and adult abdominopelvic CT based on 100 patient models," *Phys. Med. Biol.* **58**, 8755–8768 (2013).
9. X. Li et al., "Effects of protocol and obesity on dose conversion factors in adult body CT," *Med. Phys.* **39**, 6550–6571 (2012).
10. J. Sanders, L. Hurwitz, and E. Samei, "Patient-specific quantification of image quality: an automated method for measuring spatial resolution in clinical CT images," *Med. Phys.* **43**, 5330–5338 (2016).
11. Q. Fang and D. A. Boas, "Tetrahedral mesh generation from volumetric binary and gray-scale images," in *Proc. IEEE Int. Symp. Biomedical Imaging*, pp. 1142–1145 (2009).
12. "X-ray mass attenuation coefficients," in *National Institute of Standards and Technology*, http://physics.nist.gov/PhysRefData/XrayMassCoef/tab2.html (6 August 2016).
13. N. Otsu, "A threshold selection method from gray-level histograms," *IEEE Trans. Syst. Man Cybern.* **9**, 62–66 (1979).
14. NEMA XR 29-2013, "Standard attributes on CT equipment related to dose optimization and management," http://www.nema.org/Standards/Pages/Standard-Attributes-on-CT-Equipment-Related-to-Dose-Optimization-and-Management.aspx#download (25 January 2016).
15. W. Huda, K. M. Ogden, and M. R. Khorasani, "Converting dose-length product to effective dose at CT," *Radiology* **248**, 995–1003 (2008).
16. H. Schlattl et al., "Dose conversion coefficients for paediatric CT examinations with automatic tube current modulation," *Phys. Med. Biol.* **57**, 6309–6326 (2012).
17. N. Keat, "Report 05016 CT Scanner automatic exposure control systems," *London ImPACT*, http://www.impactscan.org/reports/Report05016.htm (25 January 2016).

Jeremiah Sanders is a doctoral student in medical physics at MD Anderson Cancer Center. He received his BS degree in aerospace engineering from the University of Texas at Arlington in 2014 and his MS degree in medical physics from Duke University in 2016. He is the author or coauthor of seven scientific publications. His current research interests include developing, validating, and implementing compressed sensing algorithms in magnetic resonance imaging.

Xiaoyu Tian is a researcher who recently graduated from the biomedical engineering department at Duke University. Her research interests include the quantification of radiation dose and image quality for x-ray CT examinations. She has published over 10 peer-reviewed papers in top radiology journals and presented at multiple international radiological conferences.

William Paul Segars is an associate professor of radiology and biomedical engineering and a member of the Carl E. Ravin Advanced Imaging Laboratories (RAILabs) at Duke University. He received his PhD in biomedical engineering from the University of North Carolina in 2001. He is among the leaders in the development of simulation tools for medical imaging research, where he has applied state-of-the-art computer graphics techniques to develop realistic anatomical and physiological models.

John Boone is a medical physicist with research, educational, and clinical responsibilities at the University of California Davis, where he is professor and vice chair (for research) of radiology and professor of biomedical engineering. His research interests include the development and deployment of tomographic breast imaging technology, radiation dose assessment using Monte Carlo techniques, and image quality and dose metric development.

Ehsan Samei is a tenured professor at Duke University, where he serves as the director of the Duke Medical Physics Graduate Program and the Clinical Imaging Physics Program. His interests include clinically relevant metrology of imaging quality and safety for optimum interpretive and quantitative performance. He strives to bridge the gap between scientific scholarship and clinical practice by meaningful realization of translational research and the actualization of clinical processes that are informed by scientific evidence.